Correlation Dimensions of Primitive Equation and Balanced Models

MILES SUNDERMEYER* AND GEOFFREY K. VALLIS

University of California, Santa Cruz, Santa Cruz, California

26 May 1992 and 17 November 1992

ABSTRACT

Low-order primitive equation and balanced models are compared by evaluating the correlation dimension of each over a range of Rossby numbers. The models are the nine-component primitive equation model of Lorenz and the corresponding three-component balance model. Both models display behavior ranging from stable fixed points and limit cycles to chaotic dynamics. At low Rossby number, the correlation dimensions of the models are (to the accuracy of the calculation) very similar, even in the presence of strange attractors. At higher Rossby number, the behavior differs: in some regions where the balance model goes into a limit cycle the primitive equation model displays chaotic behavior, with a correlation dimension greater than three. This appears to be caused by the (somewhat intermittent) appearance of gravity waves. Since here the calculated correlation dimension is higher than the number of slow modes, the gravity waves cannot be slaved to the slower geostrophic activity.

1. Introduction

The dynamics of the midlatitude troposphere are characterized by a low Rossby number and by stable stratification. These features naturally invite attempts to construct models that a priori incorporate such structure and are in some sense simpler than the primitive equations. Such models, normally (but not always) constructed by asymptotic methods, include quasigeostrophy, semigeostrophy, and various flavors of "balanced models." These normally filter gravity waves and are analytically as well as computationally more tractable than primitive equation models and, therefore, allow a great deal more insight into the dynamics than is possible using primitive models. Indeed this, rather than the computational advantages, is perhaps why they are so attractive. For although semi-implicit methods for the primitive equations can be computationally very efficient, clearly much of the development of the theory of baroclinic instability would have been impossible without simpler models.

Nevertheless, the accuracy of such models is of obvious importance, since a simple but incorrect model is of no use. Indeed, various studies have from time to time been done to investigate primitive equation models (PE) and a variety of intermediate models (e.g., Gent and McWilliams 1982; Curry and Winsand 1986; Allen et al. 1990). In these studies various comparisons were made between primitive equation (typically shallow water) models and the corresponding intermediate models. A common conclusion is that the balanced equation (BE) model performs as well as any of the other intermediate models examined and, over a broad range of conditions at low to medium Rossby number, is quantitatively similar to the corresponding PE model.

"Accuracy" should, of course, not only entail how well a model reproduces various known steady or exact solutions to the equations, but whether the model can qualitatively reproduce the behavior of primitive equation models under a wide range of conditions, including unsteady and highly nonlinear flow. The accurate reproduction of the nonlinear transport of heat and momentum through the growth and equilibration of a baroclinic eddy would be one such test. When a fluid is undergoing turbulent, or at least chaotic, motion, however, it can be rather difficult to compare two models. Certainly they cannot be quantitatively similar in detail, for the lack of predictability will soon destroy that. Rather, one may at the very least require that the shape of their strange attractors be similar, and a necessary condition for that is that their fractal dimensions be similar.

To this end, we compare the correlation dimensions of the attractors of a primitive equation model and a corresponding balanced model. The models used are the low-order shallow water model of Lorenz (1980) (his nine-component model) and the corresponding balanced model, first derived by Gent and McWilliams (1982, henceforth GM). [See also Vautard and Legras (1986) for a preliminary investigation of fractal dimension of the Lorenz (1980) model.] Very long integrations of both may be performed, enabling rather robust dimension calculations. The calculation of di-

* *Current affiliation:* Department of Earth, Planetary and Atmospheric Sciences, Massachusetts Institute of Technology.

Corresponding author address: Dr. Geoffrey K. Vallis, Marine Science Department and Institute of Nonlinear Science, University of California, Santa Cruz, CA 95064.

mension in a higher-order model would naturally be of interest. However, since the purpose of this study is to ascertain whether independent degrees of freedom corresponding to gravity wave activity exist, it was deemed appropriate to use the simplest models available, not only enabling the highest accuracy to be achieved in the calculations but enabling the results to be interpreted unambiguously. For example, in a pair of high-order primitive and balanced models, even if independent gravity wave modes are excited in the primitive equation model, the dimension of its attractor may still be less than the possible number of degrees of freedom of the balanced model, and hence a dimension calculation could not definitively reveal the presence of independent fast modes.

In this note, we describe the integrations of both models and the results of a calculation of their correlation dimension over a range of forcing strengths. In section 2, we describe the models and in section 3 the algorithms used to calculate dimension. In section 4, the results are given, and section 5 concludes.

2. The dynamical models

a. The continuous models

The PE model is based on the shallow-water equations over topography. The governing equations are

$$\frac{\partial \mathbf{V}}{\partial t} = -(\mathbf{V}\cdot\nabla)\mathbf{V} - f\mathbf{k}\times\mathbf{V} - g\nabla z + \nu\nabla^2\mathbf{V}, \quad (2.1)$$

$$\frac{\partial z}{\partial t} = -(\mathbf{V}\cdot\nabla)(z-h) - (H+z-h)\nabla\cdot\mathbf{V} + \kappa\nabla^2 z + F, \quad (2.2)$$

where f is a constant Coriolis parameter, $\mathbf{V}$ and z are the velocity and height fields, H is the average depth, and h is bottom topography. Both velocity and height fields are damped diffusively with coefficients ν and κ, and the system is forced by a mass source and sink $F(r)$.

Introducing a velocity potential χ and a streamfunction ψ, the horizontal velocity can be expressed as $\mathbf{V} = \nabla\chi + \mathbf{k}\times\nabla\psi$. The divergence $\nabla^2\chi$ and vorticity $\nabla^2\psi$ equations can then be found along with the corresponding height equation to make up the continuous PE model (see Lorenz 1980). The BE model is obtained by eliminating all terms containing χ in the divergence equation, giving

$$\nabla\cdot(\nabla^2\psi\nabla\psi) - \frac{1}{2}\nabla^2(\nabla\psi\cdot\nabla\psi) + f\nabla^2\psi = g\nabla^2 z. \quad (2.3)$$

The vorticity and height equations are unaltered.

b. Low-order models

The low-order models consist of spectral representations of the continuous PE and BE models truncated to a single triad of wavevectors. Denoting its members with the indices (i, j, k), the truncated nondimensional primitive equations are then given by the nine ODEs (Lorenz 1980):

$$\frac{a_i dx_i}{d\tau} = a_i b_i x_j x_k - c(a_i - a_k)x_j y_k + c(a_i - a_j)y_j x_k - 2c^2 y_j y_k - \nu_0 a_i^2 x_i + a_i y_i - a_i z_i, \quad (2.4)$$

$$\frac{a_i dy_i}{d\tau} = -a_k b_k x_j y_k - a_j b_j y_j x_k + c(a_k - a_j)y_j y_k - a_i x_i - \nu_0 a_i^2 y_i, \quad (2.5)$$

$$\frac{dz_i}{d\tau} = -b_k x_j(z_k - h_k) - b_j(z_j - h_j)x_k + cy_j(z_k - h_k) - c(z_j - h_j)y_k + g_0 a_i x_i - \kappa_0 a_i z_i + F_i. \quad (2.6)$$

The indices (i, j, k) cyclically take the values $(1, 2, 3)$. The nondimensional parameters appearing here are

$$\left.\begin{aligned} t &= f^{-1}\tau \\ \chi &= 2L^2 f \Sigma x_i\phi_i \\ \psi &= 2L^2 f \Sigma y_i\phi_i \\ z &= 2L^2 f^2 g^{-1}\Sigma h_i\phi_i \\ F &= 2L^2 f^3 g^{-1}\Sigma F_i\phi_i \\ \nu_0 &= L^{-2} f^{-1}\nu \\ \kappa_0 &= L^2 f^{-1}\kappa \\ g_0 &= HL^{-2} f^{-2} g \end{aligned}\right\}, \quad (2.7)$$

where all summations run from 1 to 3.

The low-order BE model is obtained in a similar manner as the PE but using the new divergence equation (2.3). The result is the diagnostic equation

$$a_i y_i - 2c^2 y_j y_k = a_i z_i, \quad (2.8)$$

along with equations (2.5)–(2.6). [Equation (2.8) can be obtained directly from (2.4) by eliminating all terms involving x_i.]

3. The correlation dimension

Generally speaking, the fractal dimension provides a measure of the number of independent modes excited by the system, that is, it gives the minimum number of coupled nonlinear ODEs necessary to describe the system (e.g., Mayer-Kress 1987). Typically, the fractal dimension, d, satisfies a relation of the form

$$N(r) \sim r^d \quad \text{as} \quad r \to 0, \quad (3.1)$$

where r is the edge length of an n-dimensional cube, and $N(r)$ counts the number of points on the attractor that are inside a given sized cube. For different fractal dimensions, the exact form of $N(r)$ (that is, the method of box counting) varies.

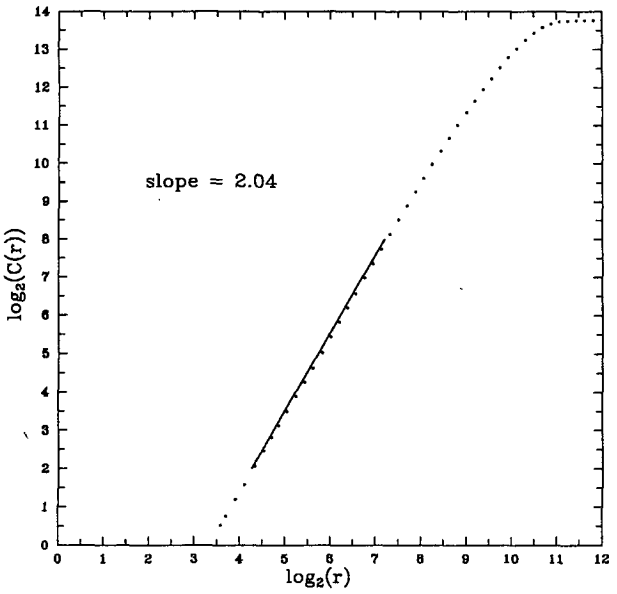

FIG. 1. Plot of $\log_2 C(r)$ vs $\log_2 r$ for the PE model for $F_1 = 0.08$ using $N_{\text{ref}} = 150$ and $N_{\text{data}} = 15\,000$. Note that for lower values of r, external noise and the finite resolution of sampled points can cause inaccuracies in the slope of the curve (although such affects are not apparent in this figure), while for higher r, the curve levels off due to geometrical effects (see text).

In the case of the correlation dimension, ν, (3.1) becomes

$$C(r) \sim r^{\nu} \quad \text{as} \quad r \to 0. \tag{3.2}$$

Here $C(r)$, known as the correlation *integral*, is given by

$$C(r) = \lim_{N\to\infty} \frac{1}{N^2} \sum_{i,j=1}^{N} \theta(r - |\vec{X}_i - \vec{X}_j|), \tag{3.3}$$

where $\theta(x)$ is the Heaviside function defined as

$$\theta(x) = \begin{cases} 1 & \text{for positive } x, \\ 0 & \text{otherwise,} \end{cases} \tag{3.4}$$

and N denotes the total number of points $\vec{X}_i$ ($i = \{1, 2, 3, \cdots, N\}$) in n-dimensional phase space used to represent the attractor (e.g., Lauterborn and Holzfuss 1986). It can be shown that the correlation dimension serves as a lower bound for the Hausdorff dimension (Grassberger and Procaccia 1983).

An efficient algorithm for calculating ν is described by Grassberger and Procaccia (1983). The method approximates $C(r)$ [see (3.3)] as

$$C(r) = \lim_{N_{\text{data}}\to\infty} \frac{1}{N_{\text{ref}}} \sum_{j=1}^{N_{\text{ref}}} \times \left(\frac{1}{N_{\text{data}}} \sum_{i=1}^{N_{\text{data}}} \theta(r - |\vec{X}_i - \vec{X}_j|) \right), \tag{3.5}$$

where N_{data} is the number of data vectors $\vec{X}_i$, and N_{ref} is the number of reference vectors $\vec{X}_j$ (see also Mayer-Kress 1987). Equation (3.5) differs from (3.3) in that the double summation has been separated into individual summations over the reference vectors and data vectors. The algorithm uses the fast convergence of the limit as $N_{\text{ref}} \to \infty$ to justify a finite summation over N_{ref} in the calculation of $C(r)$. Typically, $N_{\text{ref}} \ll N_{\text{data}}$.

Once $C(r)$ has been calculated for a number of different r, ν is found with the help of (3.2) by plotting $\log_2 r$ versus $\log_2 C(r)$. Figure 1 shows an example of such a plot for the PE model, where $F_1 = 0.08$ using $N_{\text{ref}} = 150$ and $N_{\text{data}} = 15\,000$. For higher values of r, $C(r)$ levels off due to geometrical effects; that is, r is so large that the distance calculations in (3.5) exceed the boundaries of the attractor. Also, for lower values of r, external noise and the finite resolution of sampled points cause inaccuracies in $C(r)$ (e.g., Holzfuss and Mayer-Kress 1986). It is thus preferable, for any given dataset, to use intermediate values of r when calculating ν.

4. Model comparisons

a. Numerical methods of solution

All parameter values were held fixed throughout our analysis with the exception of the forcing parameter

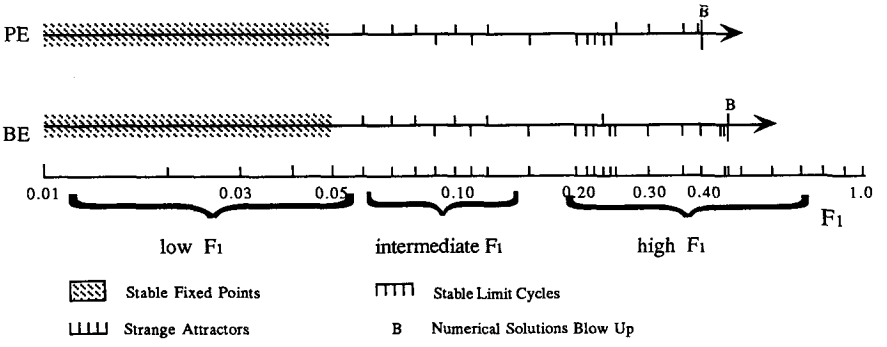

FIG. 2. Type of attractors found at different forcing values in the PE and BE models for initial conditions close to the Hadley solution.

F_1, which had values chosen along the interval [0.01, 0.50]. Strictly, simply taking $F_1 \to 0$ does not produce the quasigeostrophic limit. This is achieved by taking ν, the topography, and the Rossby number, and hence the forcing, to zero simultaneously. A bifurcation sequence produced this way could be different from simply varying the forcing parameter F_1. However, for simplicity we prefer the latter course. Apart from F_1, the parameters were given the values chosen by Lorenz (1980), namely,

$$\left.\begin{aligned} f^{-1} &= 3 \text{ h}, \quad g = 10 \text{ m s}^{-2}, \quad H = 8 \text{ km}, \\ L &= 1080 \text{ km}, \quad |h| = 2 \text{ km}, \\ \nu &= \kappa = 2.25 \times 10^6 \text{ m}^2 \text{ s}^{-1}. \end{aligned}\right\} \quad (4.1)$$

These imply a 6-day diffusive damping time for 1 and 2 subscripted variables and a 2-day damping time for subscript 3 variables. The resulting nondimensional parameters are then

$$\left.\begin{aligned} &g_0 = 8, \quad \nu_0 = \kappa_0 = \frac{1}{48}, \\ &a_1 = a_2 = 1, \quad a_3 \equiv a = 3, \\ &c^2 = a - \frac{a^2}{4} = \frac{3}{4}, \quad h_1 = -1, \\ &h_2 = h_3 = 0, \quad F_2 = F_3 = 0. \end{aligned}\right\} \quad (4.2)$$

Numerical integration of both models was done using a fourth-order Runge-Kutta stepping method and double-precision arithmetic. We used $\Delta\tau = 1/12$, that is, 15 min, which is small enough to ensure computational stability and give an accurate picture of the attractors (Lorenz 1980). Independent integrations were typically run for 2×10^6, 3.5×10^6, and 5.5×10^6 iterations for each parameter value. After discarding the first 500 000 iterations, data points were sampled every 100 time steps giving, respectively, 15 000, 30 000, and 50 000 points on the attractors. Note that the sampling frequency should be chosen long enough to produce "independent" points and that a long interval does not in any way preclude the detection of dimensions associated with motion of a higher frequency. The dimension calculation is sensitive to the space-filling properties of the motion, not its temporal frequency per se.

For the PE model, numerical integration is straightforward; all variables may simply be stepped forward in time. For the BE, integration is slightly more complicated due to the lack of a differential expression for x_i. Instead, (2.8), (2.9), and (2.11) may be manipulated to obtain a diagnostic expression for x_i (see GM). Solutions of the BE model are thus found by integrating y_i starting from some initial conditions and then computing x_i and z_i directly from y_i.

b. *Model solutions*

Models were first run starting from an initial condition chosen very close to the theoretical fixed point known as the *Hadley solution,* which lies on the attractor (Lorenz 1980). The Hadley fixed point is found for the PE model by setting

$$\left.\begin{aligned} x_1 &= -\nu_0 a_1 y_1, \\ y_1 &= F_1/a_1\nu_0(1 + a_1 g_0 + \nu_0^2 a_1^2), \\ z_1 &= (1 + \nu_0^2 a_1^2) y_1, \\ x_2 &= x_3 = y_2 = y_3 = z_1 = z_2 = 0, \end{aligned}\right\}, \quad (4.3)$$

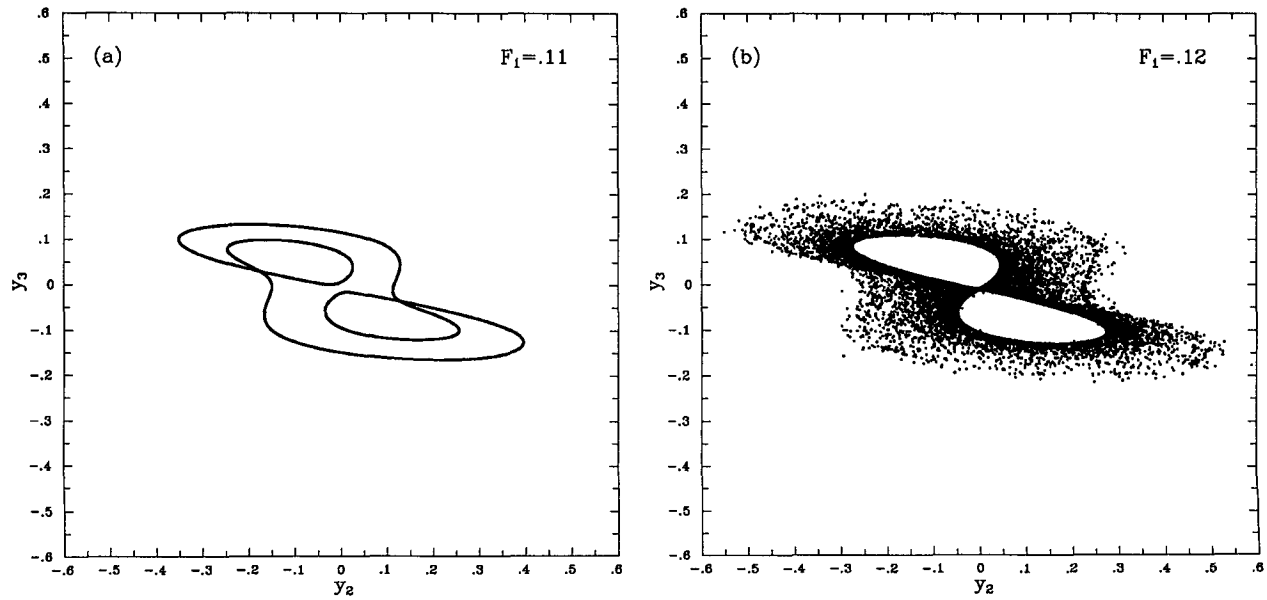

FIG. 3. Projections onto the y_2y_3 plane of points on (a) a "typical" stable limit cycle and (b) a strange attractor for the PE model. Each graph is made up of 15 000 points representing 2×10^6 iterations.

while for the BE model it is found by setting

$$\left.\begin{aligned} y_1 &= F_1/a_1\nu_0(1 + a_1 g_0), \\ y_2 &= y_3 = 0 \end{aligned}\right\} \qquad (4.4)$$

(see GM). We perturb this slightly by setting $y_2 = -z_2 = -10^{-5}$ for the PE model and $y_2 = -10^{-5}$ for the BE model. Phase space trajectories of both systems were examined as F_1 was varied between 0.01 and 0.47. Model behavior for F_1 in this range is displayed in Fig. 2, following the format of similar results of GM. For low values of F_1 on the interval [0.01, 0.05], solutions of both models converge to stable fixed points. As F_1 is increased from 0.06 to 0.12, this changes to an interleaving between stable limit cycles of various periods and strange attractors. Figures 3a and 3b show projections onto the y_2y_3 plane of points on a stable limit cycle and strange attractor that are "typical" of both the PE and BE models for this intermediate forcing range. As F_1 is increased further, BE model solutions tend primarily toward stable limit cycles. These undergo a qualitative change in shape as solutions encounter a strange attractor at $F_1 = 0.23$ (Figs. 4a,b,c). Meanwhile, the PE model, after briefly settling down to stable limit cycles, also finds strange attractors that persist above $F_1 = 0.24$. Curry and Winsand (1986) suggest that this reappearance of strange attractors in both the PE and BE models at high F_1 is the result of the same bifurcation phenomenon in each model. A visual inspection of the new PE model attractors (Fig.

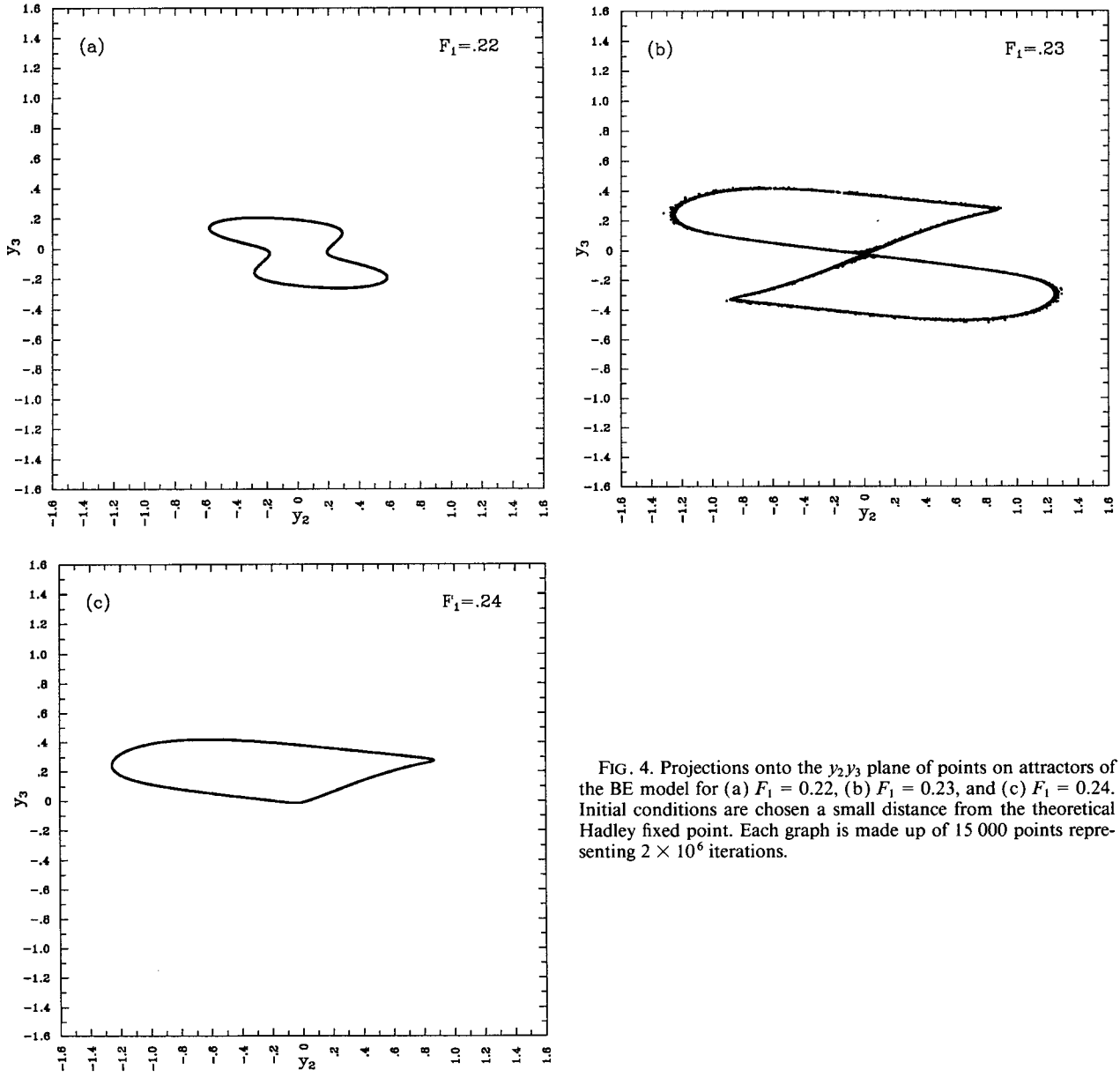

FIG. 4. Projections onto the y_2y_3 plane of points on attractors of the BE model for (a) $F_1 = 0.22$, (b) $F_1 = 0.23$, and (c) $F_1 = 0.24$. Initial conditions are chosen a small distance from the theoretical Hadley fixed point. Each graph is made up of 15 000 points representing 2×10^6 iterations.

5a) additionally shows that the qualitative shape of these strange attractors is unlike that which is typically found for lower F_1 (see Fig. 3b). Specifically, PE model solutions for high F_1 undergo intermittent large-scale oscillations, as well as small-scale "fast" ones. An example of these can be seen in Fig. 5b, which shows a time series diagram of y_3 when $F_1 = 0.25$. The obvious persistence of this "fast" motion even after large time indicates that gravity wave oscillations in the PE, at least for high Rossby number, are not a transitory phenomenon (see also Warn and Menard 1986). Finally, when forcing is increased even higher, solutions of the PE and BE models for these initial conditions blow up at $F_1 = 0.40$ and $F_1 = 0.47$, respectively. This property may be related to the fact that neither of the models conserve energy in inviscid adiabatic flow (e.g., GM).

Another initial condition used was such that all variables were set equal to 0.1. Model behavior for F_1 between 0.01 and 0.50 for this initial condition is sum-

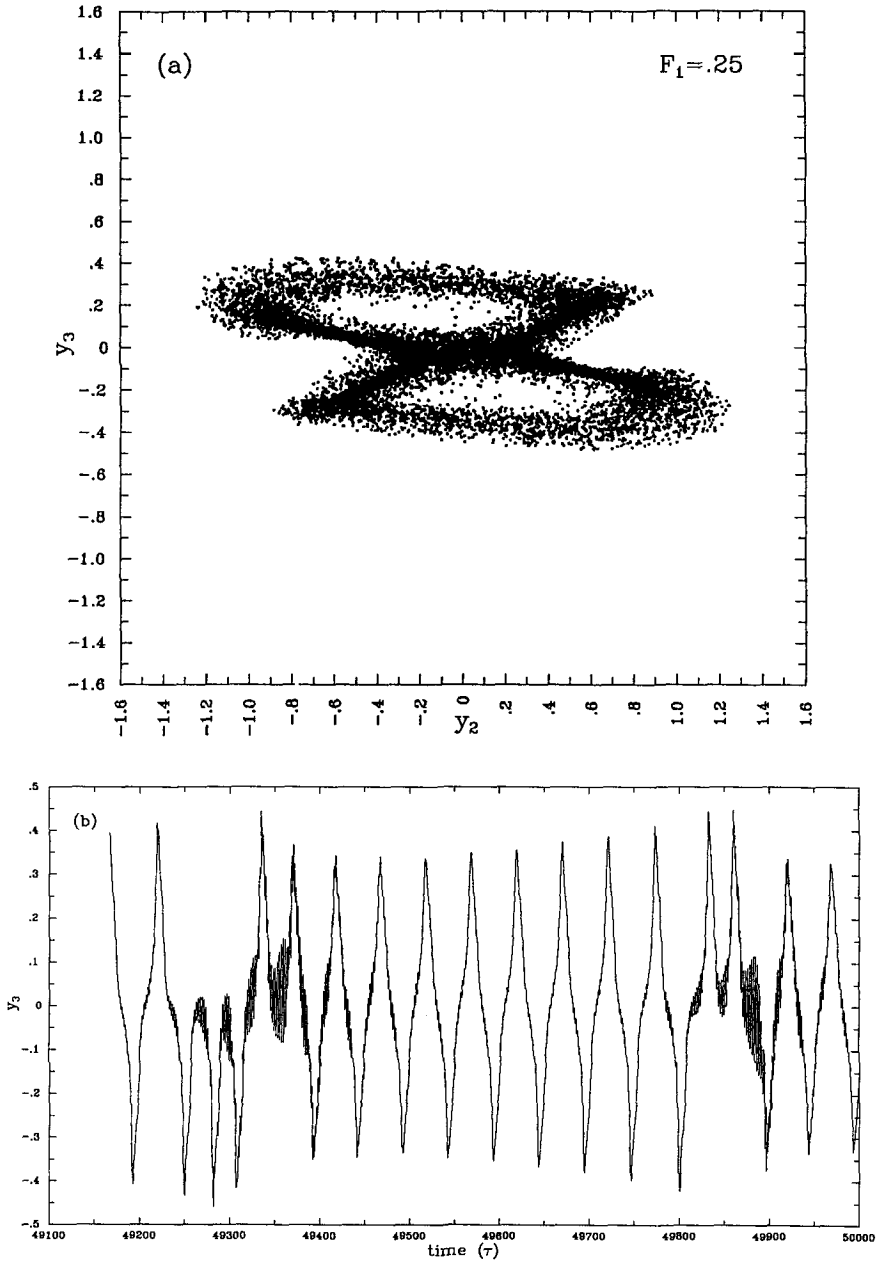

FIG. 5. Projection onto the y_2y_3 plane of points on a strange attractor (a) and a time series diagram of y_2 (b), which are characteristic of the PE model at high F_1 values. Here $F_1 = 0.25$ and initial conditions are chosen a small distance from the theoretical Hadley fixed point.

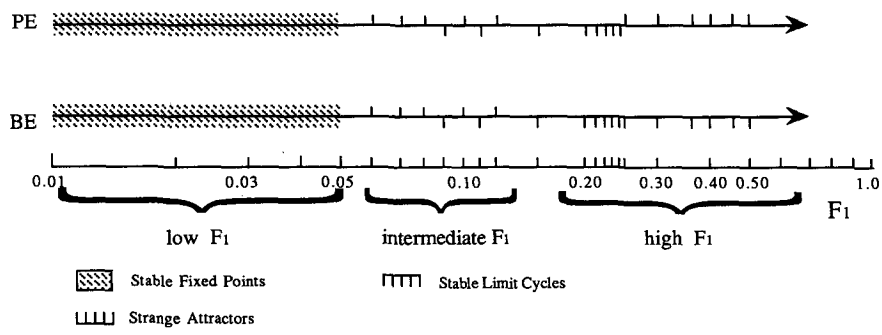

FIG. 6. Types of attractors found at different forcing values in the PE and BE models for the initial condition where all variables are set equal to 0.1.

marized in Fig. 6. Solutions behave almost identically to corresponding solutions for the previous initial condition, with a few exceptions. For low F_1, although solutions still converge to stable fixed points, another fixed point in the BE model was occasionally found. Also, while in the PE model the transition back to strange attractors at high F_1 is the same for both initial conditions, this time stable limit cycles in the BE model experience their change in shape on the interval $0.24 \leqslant F_1 \leqslant 0.25$ rather than the interval $0.22 \leqslant F_1 \leqslant 0.24$. Finally, neither model blows up for values of F_1 as high as 0.50.

c. *The correlation dimension*

The correlation dimension, ν, was calculated as in section 3. Specifically, we used the algorithms of Lauterborn and Holzfuss (1986) and Holzfuss and Mayer-Kress (1986), which implement the method described by Grassberger and Procaccia (1983) for calculating $C(r)$. After plotting $\log_2 r$ versus $\log_2 C(r)$, a least squares method was used to fit values of $\log_2 C(r)$ to a straight line, the slope of which equals ν.

For each model, $C(r)$ was computed using 150 reference vectors (N_{ref}) with 15 000, 30 000, and 50 000 data vectors (N_{data}) from initial conditions with all variables equal to 0.1. The resulting values of ν for F_1 between 0.01 and 0.50 for the PE and BE models are graphed in Figs. 7 and 8. The fact that the calculated value of ν did not significantly depend on the number of data vectors used suggests that the number of points used to represent the attractors was sufficient. Tests using 300 and 500 reference vectors also suggested the same for the number of reference vectors used.

Comparing Figs. 7 and 8, one clearly sees the similarities in the behavior of the attractors of both systems for F_1 on the interval [0.01, 0.24]. As F_1 increases above 0.25, however, the change in the behavior in the PE model is also quite apparent. In particular, the presence of small-scale gravity waves in the PE model results in a significantly higher value of the correlation dimension. The fact that for high F_1 the correlation dimension for the PE model is consistently greater than three implies that for higher values of forcing, the number of independent modes excited in the PE system is greater than three. For the BE model, however, ν, and thus the number of excited modes, is, and by virtue of the model must always be, less than three. More generally, our comparison shows that for $F_1 \leqslant 0.24$ the BE model is in close agreement with the PE model, while for $F_1 \geqslant 0.25$ it is in disagreement.

5. Discussion

The question at hand was whether the PE model contained unexcited degrees of freedom and could therefore be approximated by a smaller number of ODEs, in particular the BE model. The results of our

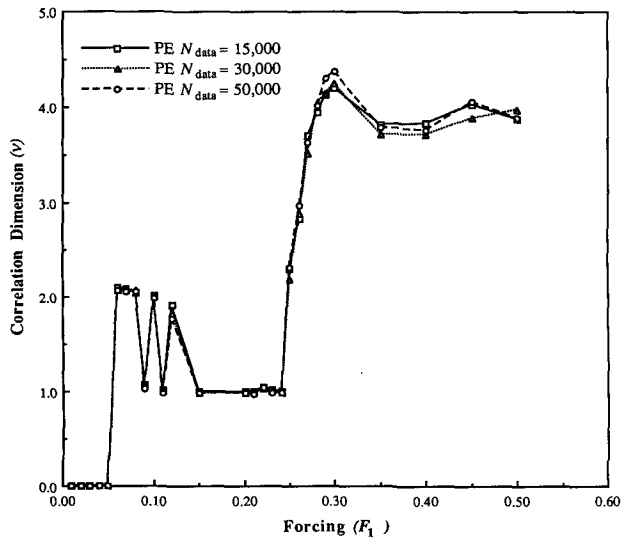

FIG. 7. Correlation dimension as a function of forcing intensity, F_1, for attractors of the PE model with $C(r)$ computed using $N_{\text{ref}} = 150$ and $N_{\text{data}} = 15\,000$, 30 000, and 50 000. Initial conditions are such that all variables are set equal to 0.1. Note that although points are connected in our graph, this does not imply that the values of the correlation dimension change in a continuous manner, and F_1 values that are not explicitly plotted here cannot necessarily be interpolated from values that are.

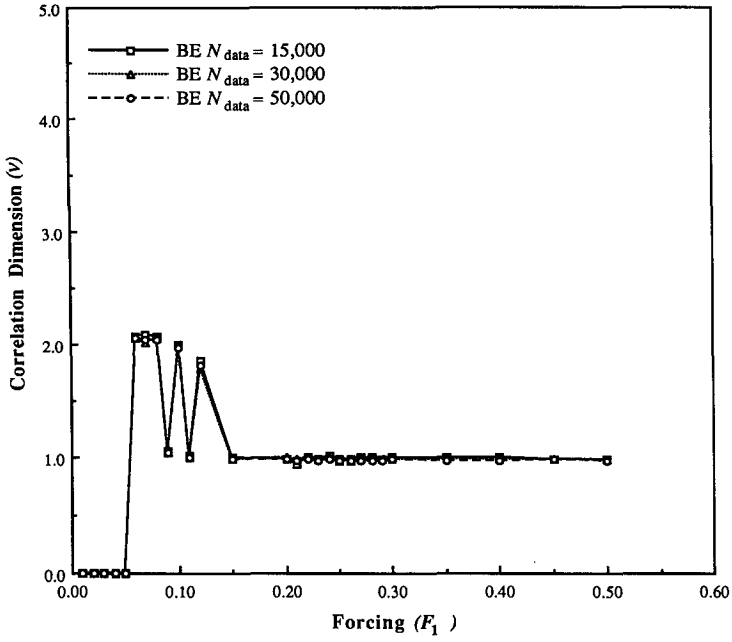

FIG. 8. As in Fig. 7 for BE model.

analysis can be interpreted as follows: for low to intermediate forcing ($0.01 \leq F_1 \leq 0.24$) the BE model seems to be an excellent approximation of the PE model. Not only do both models possess the same types of attractors for like values of F_1, but the shapes and the correlation dimensions, ν, of these attractors closely correspond. For higher forcing ($F_1 \geq 0.25$), however, there are substantial differences between the behavior of the PE and BE models (Fig. 9). Namely, the PE model possesses strange attractors with $\nu > 3$, while BE solutions tend to stable limit cycles with $\nu = 1$. The high dimension of the PE attractors is evidently due to intermittent bursts of small-scale gravity wave oscillations, which raise the number of excited degrees of freedom in the system. These small-scale oscillations are detected only as transient phenomena for lower F_1 in the PE model and are always nonexistent in the BE model, thus resulting in lower dimension attractors in both cases.

For $F_1 \geq 0.25$, the BE model is evidently *not* a good approximation of the PE model because it is limited to possessing attractors for which $\nu \leq 3$, whereas the PE model possesses attractors for which $\nu > 3$ (whether the PE can be approximated by some other low-order system possessing less than nine degrees of freedom remains open). The onset of gravity wave activity in this model is rather sudden; it would be of interest to determine whether this feature also occurs in high-order PE models or if this behavior is an artifact of the low-order truncation. Note, however, that this activity points to a difference between a PE model and *any* balance model. Even a higher-order balance model, if indeed balanced, would be unable to capture such phenomena and display a correlation dimension higher than the number of slow modes (three in this case).

For small forcing (and therefore small Rossby number), the BE model is clearly a good approximation. Care should be taken, however, in interpreting our results as implying the existence of a true slow manifold. Warn and Menard (1986) found that even at small values of Rossby number gravity waves existed. Although these were of exceedingly small amplitude, sometimes up to 10^{13} times smaller than the slow motion, if they are truly independent of the slow motion, then as real degrees of freedom they would still add to

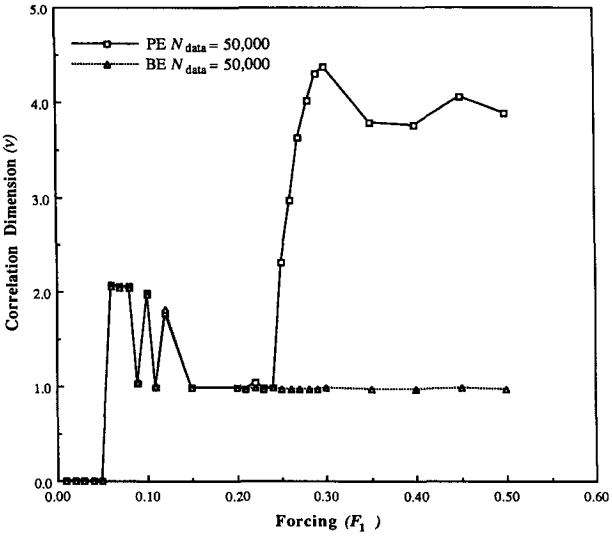

FIG. 9. Superposition of correlation dimension vs F_1 graphs for attractors of the PE and BE model using the initial condition where all variables are set equal to 0.1 (only ν computed with N_{data} = 50 000 are plotted).

the dimension of the attractor. This would appear in the calculations as a second scaling range at small values of r in plots such as Fig. 1. To actually include these effects in an accurate computation of the dimension of the attractor would, however, require extremely high precision and an extremely long integration and is unfortunately not feasible nor even approachable. Our calculations will detect fast motion of amplitudes down three or four orders of magnitude smaller than the slow motion, so they cannot resolve the small amplitudes detected by Warn and Menard. It may be possible to improve accuracy more efficiently than simply counting more points on the attractor by first subtracting the balanced signal from the total signal and then computing the dimensionality of the remainder, in a similar manner to the way Warn and Menard first deduced the presence of small-amplitude gravity waves. It is not clear, however, whether such a procedure would yield accurate estimates of the total dimensionality since once the balanced signal has been subtracted off, it is not obvious how the independence of any remaining fast motion could be ascertained.

Finally, our integrations unambiguously do not find a slow manifold at higher Rossby numbers. Although it remains a possibility that one exists in the close neighborhood of the actual system trajectory, it seems unlikely that it is an attracting manifold since there is no evidence that the gravity wave oscillations become weaker over time.

Acknowledgments. This work was funded by the NSF (ATM 8914004) and the ONR (N00014-90-J-1618). We are grateful to Peter Gent and, especially, Tom Warn for their comments and to G. Mayer-Kress for some dimensionality codes.

REFERENCES

Allen, J. S., J. Barth, and P. Newberger, 1990: On intermediate models for barotropic continental shelf and slope flow fields. Part I: Formulation and comparison of exact solutions. *J. Phys. Oceanogr.*, **20,** 1017–1042.

Curry, J. H., and D. Winsand, 1986: Low-order intermediate models: Bifurcation, recurrence, and solvability. *J. Atmos. Sci.*, **43,** 2360–2373.

Gent, P. R., and J. C. McWilliams, 1982: Intermediate model solutions to the Lorenz equations: Strange attractors and other phenomena. *J. Atmos. Sci.*, **39,** 3–13.

Grassberger, P., and I. Procaccia, 1983: Characterization of strange attractors. *Phys. Rev. Lett.*, **50,** 346–349.

Holzfuss, J., and G. Mayer-Kress, 1986: An approach to error-estimation in the application of dimension algorithms. *Dimensions and Entropies in Chaotic System—Quantification of Complex Behaviour,* G. Mayer-Kress, Ed., Springer-Verlag, 114–122.

Lauterborn, W., and J. Holzfuss, 1986: Evidence for a low-dimensional strange attractor in acoustic turbulence. *Phys. Lett. A,* **115,** 369–372.

Lorenz, E. N., 1980: Attractor sets and quasigeostrophic equilibrium. *J. Atmos. Sci.*, **37,** 1685–1699.

Mayer-Kress, G., 1987: Application of dimension algorithms to experimental chaos. *Directions in Chaos,* Hao Bai-lin, Ed., World Scientific, 122–147.

Vautard, R., and B. Legras, 1986: Invariant manifolds, quasi-geostrophy, and initialization. *J. Atmos. Sci.*, **43,** 565–584.

Warn, T., and R. Menard, 1986: Nonlinear balance and gravity-inertial wave saturation in a simple atmospheric model. *Tellus,* **38A,** 285–294.